Acta Crystallographica Section B
Structural Science
ISSN 0108-7681

Low-temperature phase transition in glycine–glutaric acid co-crystals studied by single-crystal X-ray diffraction, Raman spectroscopy and differential scanning calorimetry

Boris A. Zakharov,[a,b]* Evgeniy A. Losev,[a,b] Boris A. Kolesov,[b,c] Valeri A. Drebushchak[b,d] and Elena V. Boldyreva[a,b]*

[a]Institute of Solid State Chemistry and Mechanochemistry SB RAS, Novosibirsk, Russian Federation, [b]REC-008 Novosibirsk State University, Novosibirsk, Russian Federation, [c]Institute of Inorganic Chemistry SB RAS, Novosibirsk, Russian Federation, and [d]Institute of Geology and Mineralogy SB RAS, Russian Federation

Correspondence e-mail: b.zakharov@yahoo.com, eboldyreva@yahoo.com

Received 31 January 2012
Accepted 12 April 2012

The occurrence of a first-order reversible phase transition in glycine–glutaric acid co-crystals at 220–230 K has been confirmed by three different techniques – single-crystal X-ray diffraction, polarized Raman spectroscopy and differential scanning calorimetry. The most interesting feature of this phase transition is that every second glutaric acid molecule changes its conformation, and this fact results in the space-group symmetry change from $P2_1/c$ to $P\bar{1}$. The topology of the hydrogen-bonded motifs remains almost the same and hydrogen bonds do not switch to other atoms, although the hydrogen bond lengths do change and some of the bonds become inequivalent.

1. Introduction

Multicomponent crystals with components which are present in a well defined stoichiometric ratio (salts and co-crystals) attract much attention. They are promising as new materials with non-linear optical properties (Fleck & Petrosyan, 2010), or as new forms of pharmaceuticals for solid dosage forms with improved dissolution kinetics or shelf-life (Sekhon, 2009; Shan & Zaworotko, 2008). The components in a co-crystal assemble *via* non-covalent interactions, such as hydrogen bonds, π–π or van der Waals interactions (Sekhon, 2009). Studies of co-crystals are also interesting to improve our understanding of factors determining the formation of a crystal structure and its variation *versus* temperature and pressure. Salts and co-crystals may be distinguished by the absence of proton transfer between components in co-crystals (Childs *et al.*, 2007), but there is no sharp borderline between the two types of multicomponent crystals since a molecular co-crystal can transform (continuously or sharply) into a salt on variations in temperature (Asaji *et al.*, 2007; Grobelny *et al.*, 2011; Majerz *et al.*, 1997) or pressure (Casati *et al.*, 2009).

Amino acids are known to form salts with carboxylic acids much more often than co-crystals. Glycine normally forms salts with carboxylic acids, see, for instance, the Cambridge Structural Database (CSD; Allen, 2002) refcodes WOVYOV (Subha Nandhini *et al.*, 2001), WOVYOV01 (Tumanov *et al.*, 2010), WEHZAL (Chitra *et al.*, 2006), RENBAN (Rajagopal *et al.*, 2001), AWIHIY (Losev *et al.*, 2011) *etc.*, with the exception of fumaric acid monohydrate (molar ratio glycine: fumaric acid: water is 2:1:1, refcode GOLZIR; Natarajan *et al.*, 2009), where glycine is present both in the zwitterionic and the protonated form. The glycine–glutaric acid co-crystal is the only known co-crystal of an amino acid with glutaric acid. Interestingly enough, this new structure has been obtained and described independently very recently by two research groups (Losev *et al.*, 2011; Riscob *et al.*, 2011). It crystallizes well as large perfect crystals and has pronounced non-linear

optical properties (Riscob *et al.*, 2011). Knowledge of the response of the crystal structure to variations of temperature and pressure is of interest to understanding interactions in organic crystals, and also in view of the potential applications of this co-crystal as a molecular material and a component of supramolecular devices.

The aim of the present study was to follow the structural changes in a co-crystal of glycine with glutaric acid *versus* temperature. Originally we supposed that a co-crystal–salt transition may be possible, similar to what has already been observed for other compounds (Asaji *et al.*, 2007; Grobelny *et al.*, 2011; Majerz *et al.*, 1997), but, as often happens, the real behavior of the system turned out to be quite unexpected and more complex. The molecules of glutaric acid remained non-ionized in the temperature range from ambient down to 100 K. Instead of the expected 'co-crystal to salt' transition, a conformational polymorphic transformation with a change in space-symmetry group and doubling of Z' has been observed at 220–230 K. The topology of the hydrogen-bond network was basically preserved, although the lengths of all the N—H···O and some of the O—H···O hydrogen bonds have changed.

2. Experimental

2.1. Samples

Co-crystals of glycine with glutaric acid were grown by slow evaporation at room temperature of aqueous solution (*ca* 5 ml) containing stoichiometric amounts (1:1) of glycine (Reaktiv, Russia, 98% grade) and glutaric acid (Sigma-Aldrich, GmbH, Germany, 99% grade).

2.2. Single-crystal X-ray diffraction

Variable-temperature single-crystal X-ray diffraction was carried out using a Stoe IPDS-2 diffractometer with an image-plate detector, graphite monochromator, Mo $K\alpha$ radiation and an Oxford Cryostream cooling device. The cooling rate was ~ 100 K h^{-1}. Originally we planned to cool the sample down from 300 to 100 K in 25 K steps and after that to heat it up in a similar way up to 300 K. A transition from one temperature point to another usually took approximately 20–25 min. A crystal was cooled from ambient temperature (300 K) down to 200 K, and at this point the crystal fell down from the glass rod holder (most likely because of a phase transition) when we attempted to collect diffraction data at 200 K. We had to repeat the experiment with a new crystal, this time fixed at a Mitigen holder with cryo-oil. The data for the new crystal have been collected at 300 K and agreed very well with the data set collected for the first sample. Single-crystal diffraction data for the low-temperature phase (II) at 200 K and below were then collected using the second crystal.

Parameters characterizing data collection and refinement as well as crystal data are summarized in Table 1. *X-AREA* (Stoe & Cie, 2006) and *X-RED*32 (Stoe & Cie, 2006) was used for cell refinement, data collection and data reduction. Crystal structures were solved by direct methods using *SHELXS*97 (Sheldrick, 2008) and refined on F^2 using *X-STEP* (Stoe & Cie, 2006) and *SHELXL*97 (Sheldrick, 2008). *Mercury* (Macrae *et al.*, 2008) and *PLATON* (Spek, 2009) were used for visualization, finding molecular graphs and analysis of structure motifs. CIF files were prepared for publication using *enCIFer* (Allen *et al.*, 2004). *Tensor* (Hazen & Finger, 1982) was used to calculate the anisotropy of the lattice strain. As far as we could see from the X-ray data collected at 200 K and below using the second crystal fixed with oil the sample underwent a phase transition, during which time two non-merohedral domains appeared with the ratio of reflections with $I > 6\sigma \simeq 3{:}1$ at 200 K (see Fig. ESI-1 in the supplementary material[1]). The transformation matrix between orientation matrices of larger and smaller domains was (−0.9377 −0.0921 −0.3348 / −0.0923 −0.8633 0.4972 / −0.3346 0.4959 0.8011); the number of reflections from the larger domain was 11 557, and 1894 (16.4%) of them were overlapped with reflections from the smaller domain (data for T = 200 K). Interestingly, the crystal did not crack as a result of this transformation. The transition was completely reversible: when temperature was released from 100 to 300 K and data were collected at ambient conditions, the reflections could be described by the same orientation matrix and cell parameters corresponding to phase (I) (no different domains were detected). A very small (5% at 300 K) number of reflections with $I > 6\sigma$ which did not fit this orientation matrix was practically the same before and after the phase transition and could be ascribed to X-ray scattering from cryo-oil, crystal holder, ice particles *etc.* The photographs of the crystal taken at different temperatures confirm the conclusions from X-ray diffraction data: different domains with clear borderlines can be seen in phase (II) at 200 K (see Fig. ESI-2 in the supplementary material). The crystal structure was solved and refined using non-overlapping reflections from the larger domain only, although data completeness in this case was $\sim 85\%$ despite having optimized the data collection strategy for a triclinic cell since overlapping reflections have been removed from the HKLF4 dataset for the larger component. Of course we tried to refine the structure also using the complete dataset and the HKLF5 *SHELXL* format and the structural model was essentially the same, but the resulting quality of the displacement ellipsoids was lower. So we made our final choice using only one set of reflections and refining the crystal structure using the HKLF4 format. All H atoms were located in difference-Fourier maps; H-atom parameters were treated as follows: (*a*) HFIX 137 was used to refine torsion angles in idealized NH_3 groups allowing them to rotate but not to tip, (*b*) CH_2 groups were refined using a riding model with H—C—H tetrahedral angles by HFIX 23, (*c*) OH groups were treated performing rigid-group refinement with tetrahedral C—O—H angles by HFIX 147.

In a special separate experiment with another crystal, we tested whether consecutive occurrences of the transitions may induce crystal damage over time. The same crystal was

[1] Supplementary data for this paper are available from the IUCr electronic archives (Reference: GP5050). Services for accessing these data are described at the back of the journal.

Table 1
Experimental details of low-temperature single-crystal X-ray diffraction data collection and refinement for a glycine–glutaric acid co-crystal.

For all structures: $C_5H_8O_4{\cdot}C_2H_5NO_2$, M_r = 207.18, Z = 4. Experiments were carried out with Mo $K\alpha$ radiation using a Stoe IPDS-2 diffractometer. Refinement was with 0 restraints. H-atom parameters were constrained.

	300 K	275 K	250 K	225 K	200 K
Crystal data					
Crystal system, space group	Monoclinic, $P2_1/c$, Phase (I)	Monoclinic, $P2_1/c$, Phase (I)	Monoclinic, $P2_1/c$, Phase (I)	Monoclinic, $P2_1/c$, Phase (I)	Triclinic, $P\bar{1}$, Phase (II)
Temperature (K)	300	275	250	225	200
a, b, c (Å)	4.9110 (7), 20.922 (3), 10.2744 (15)	4.9022 (7), 20.901 (3), 10.2730 (15)	4.8960 (6), 20.878 (2), 10.2701 (13)	4.8888 (6), 20.859 (2), 10.2664 (13)	4.9155 (7), 20.215 (3), 10.1862 (16)
α, β, γ (°)	90, 114.586 (10), 90	90, 114.60 (1), 90	90, 114.634 (9), 90	90, 114.648 (9), 90	85.578 (14), 113.133 (11), 88.301 (13)
V (Å^3)	959.9 (2)	957.0 (2)	954.3 (2)	951.6 (2)	926.1 (2)
No. of reflections for cell measurement	3307	3205	3499	3782	6919
θ range (°) for cell measurement	2.0–29.2	2.0–29.2	2.0–29.5	2.0–29.5	2.0–29.6
μ (mm^{-1})	0.13	0.13	0.13	0.13	0.13
Crystal size (mm)	0.32 × 0.17 × 0.10	0.32 × 0.17 × 0.10	0.32 × 0.17 × 0.10	0.32 × 0.17 × 0.10	0.40 × 0.23 × 0.10
Data collection					
No. of measured, independent and observed [$I > 2\sigma(I)$] reflections	6828, 2578, 1421	6792, 2570, 1461	6775, 2562, 1535	6775, 2558, 1594	9663, 4312, 2491
R_{int}	0.046	0.047	0.045	0.043	0.055
θ values (°)	θ_{max} = 29.2, θ_{min} = 2.0	θ_{max} = 29.2, θ_{min} = 2.0	θ_{max} = 29.2, θ_{min} = 2.0	θ_{max} = 29.2, θ_{min} = 2.0	θ_{max} = 29.2, θ_{min} = 2.0
(sin $\theta/\lambda)_{max}$ (Å^{-1})	0.686	0.687	0.686	0.686	0.686
Range of h, k, l	$h = -5 \rightarrow 6$, $k = -28 \rightarrow 24$, $l = -14 \rightarrow 14$	$h = -5 \rightarrow 6$, $k = -28 \rightarrow 24$, $l = -14 \rightarrow 14$	$h = -5 \rightarrow 6$, $k = -28 \rightarrow 24$, $l = -14 \rightarrow 14$	$h = -5 \rightarrow 6$, $k = -28 \rightarrow 24$, $l = -14 \rightarrow 14$	$h = -6 \rightarrow 5$, $k = -27 \rightarrow 27$, $l = -13 \rightarrow 13$
Refinement					
$R[F^2 > 2\sigma(F^2)]$, $wR(F^2)$, S	0.048, 0.096, 0.89	0.043, 0.085, 0.87	0.044, 0.086, 0.88	0.042, 0.081, 0.88	0.049, 0.081, 0.89
No. of reflections	2578	2570	2562	2558	4312
No. of parameters	130	130	130	130	259
$\Delta\rho_{max}$, $\Delta\rho_{min}$ (e Å^{-3})	0.19, −0.17	0.16, −0.17	0.16, −0.20	0.21, −0.18	0.19, −0.21

	175 K	150 K	125 K	100 K
Crystal data				
Crystal system, space group	Triclinic, $P\bar{1}$, Phase (II)	Triclinic, $P\bar{1}$, Phase (II)	Triclinic, $P\bar{1}$, Phase (II)	Triclinic, $P\bar{1}$, Phase (II)
Temperature (K)	175	150	125	100
a, b, c (Å)	4.9098 (7), 20.194 (3), 10.1777 (15)	4.9021 (7), 20.167 (3), 10.1686 (15)	4.8952 (6), 20.151 (3), 10.1585 (13)	4.8884 (7), 20.136 (3), 10.1518 (15)
α, β, γ (°)	85.571 (13), 113.118 (10), 88.306 (12)	85.540 (11), 113.122 (10), 88.270 (11)	85.518 (11), 113.088 (9), 88.264 (11)	85.486 (13), 113.065 (10), 88.263 (12)
V (Å^3)	923.3 (2)	919.7 (2)	916.9 (2)	914.5 (2)
No. of reflections for cell measurement	7461	7886	8370	8917
θ range (°) for cell measurement	2.1–29.6	2.1–29.6	2.1–29.6	2.1–29.6
μ (mm^{-1})	0.13	0.13	0.13	0.13
Crystal size (mm)	0.40 × 0.23 × 0.10	0.40 × 0.23 × 0.10	0.40 × 0.23 × 0.10	0.40 × 0.23 × 0.10
Data collection				
No. of measured, independent and observed [$I > 2\sigma(I)$] reflections	9568, 4319, 2580	10 066, 4417, 2840	9997, 4391, 2935	8816, 4247, 2766
R_{int}	0.052	0.040	0.038	0.052
θ values (°)	θ_{max} = 29.2, θ_{min} = 2.0	θ_{max} = 29.2, θ_{min} = 2.0	θ_{max} = 29.2, θ_{min} = 2.0	θ_{max} = 29.2, θ_{min} = 2.0
(sin $\theta/\lambda)_{max}$ (Å^{-1})	0.687	0.686	0.686	0.686
Range of h, k, l	$h = -6 \rightarrow 5$, $k = -27 \rightarrow 27$, $l = -13 \rightarrow 13$	$h = -6 \rightarrow 5$, $k = -27 \rightarrow 27$, $l = -13 \rightarrow 13$	$h = -6 \rightarrow 5$, $k = -27 \rightarrow 27$, $l = -13 \rightarrow 13$	$h = -6 \rightarrow 5$, $k = -27 \rightarrow 27$, $l = -13 \rightarrow 13$
Refinement				
$R[F^2 > 2\sigma(F^2)]$, $wR(F^2)$, S	0.049, 0.088, 0.89	0.039, 0.077, 0.88	0.039, 0.075, 0.90	0.053, 0.097, 0.98
No. of reflections	4319	4417	4391	4247
No. of parameters	259	259	259	259
$\Delta\rho_{max}$, $\Delta\rho_{min}$ (e Å^{-3})	0.22, −0.23	0.21, −0.20	0.23, −0.20	0.31, −0.29

repeatedly cooled down from 250 to 200 K at 100 K h^{-1} and then heated back at the same rate; the total number of such cycles was equal to five. No damage of the single crystal could be observed visually. Neither did diffraction reflections broaden or split. For a selected crystal, the ratio and the mutial orientation of the components formed on cooling in several cycles were approximately the same (within the experimental error), but for different crystals they differed.

2.3. Raman spectroscopy

Single-crystal Raman spectra with a polarization vector of the incident and scattered beam directed along long, medium and short dimensions of the crystals [*ll*, *mm*, *ss* polarizations, which are related to the directions of the crystallographic axes as ***aa***, (***a*** + ***c***)(***a*** + ***c***), ***bb***] were collected using a Raman spectrometer with the charge-coupled device (CCD) detector LabRAM HR 800 from HORIBA Jobin Yvon. The lines of an Ne lamp were used for spectral calibration. The 488 nm line of an Ar^+ laser was used for spectral excitation with the diameter of the laser spot on the sample surface of 1 µm. The laser power at the sample was typically about 8 mW. The spectra at all temperatures were measured in a 180° backscattering collection geometry with a Raman microscope. The low-temperature spectra were recorded by mounting the crystal on a cold finger of a helium cryostat JANIS ST-500HT. The precision of the measured temperatures of the cold finger was 0.1 K, but the true temperature of the sample could differ from the measured one due to some heating of the sample in the laser spot. We estimate this heating as 4–5 K for transparent crystals. All measurements were performed with a spectral resolution of 2 cm^{-1}. The measurements were carried out on heating the samples from 5 K up to 300 K at 5 and 20 K and further with 20 K steps, each spectrum being measured for 5–10 min.

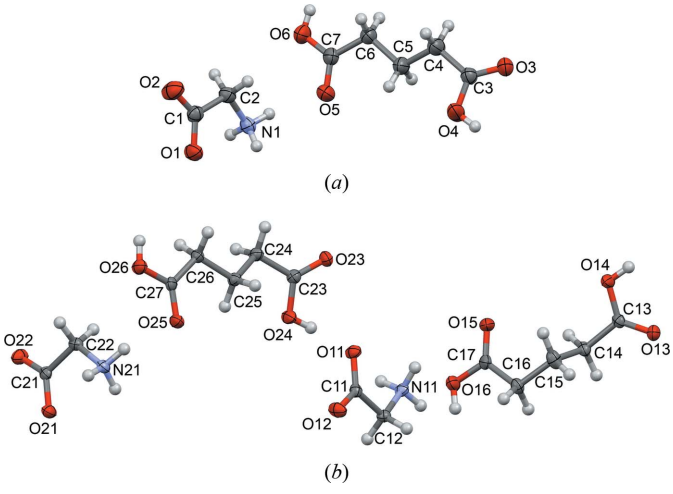

Figure 1
Displacement ellipsoid plots of glutaric acid–glycine co-crystal (*a*) phase (I) and (*b*) phase (II) showing the atom-numbering scheme and 50% probability displacement ellipsoids at 300 and 200 K, respectively. H atoms are shown as arbitrary spheres.

2.4. Differential scanning calorimetry

The thermal effects of the glycine–glutaric acid co-crystal on heating were measured using a DSC-204 calorimeter (Netzsch; standard Al crucibles; argon flow of 24 ml min^{-1}; heating rate of 6 and 3 K min^{-1}; temperature range from 145 to 300 K). Several runs with different samples after several crystallizations were performed. The results were compared, in particular, for:

(i) three single crystals very close in size that were picked up separately from the batch with tweezers (total 3.97 mg);

(ii) the powder of broken crystals that was taken from the same batch with a spatula (total 5.89 mg);

(iii) a flat single crystal after another crystallization shaped in a square $\sim 2 \times 2$ mm of 3.95 mg.

The last sample was measured in heating–cooling cycles to clarify the temperature hysteresis and mechanical stability after the phase transition.

3. Results and discussion

3.1. Single-crystal X-ray diffraction

Asymmetric units of phases (I) and (II) of the title compound are shown in Fig. 1. On cooling the crystal from ambient temperature down to 225 K, only continuous struc-

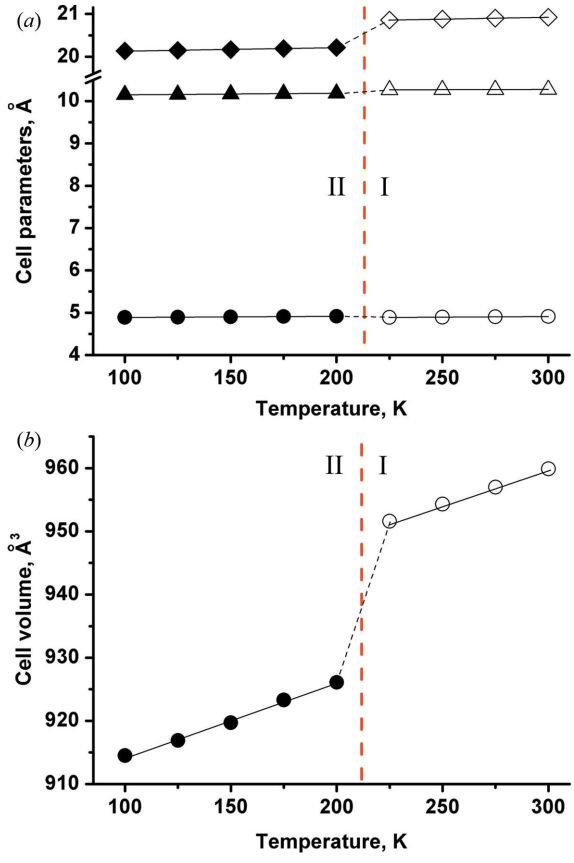

Figure 2
Changes in the cell parameters (*a*) and cell volume (*b*). Circles, rhombs and triangles define axes *a*, *b* and *c* (*a*); phase (I) – open symbols, phase (II) – filled symbols (for both figures).

Table 2
Parameters characterizing linear strain along the principal axes of strain ellipsoid for a glycine–glutaric acid co-crystal on cooling (output data of *Tensor*; Hazen & Finger, 1982).

	Angle with		
	+*A* (Error)	+*B* (Error)	+*C* (Error)
Phase (I) (300–225 K)			
Axis 1	110 (1)	90 (0)	4 (1)
Axis 2	90 (0)	0 (0)	90 (0)
Axis 3	20 (1)	90 (0)	94 (1)
Phase (II) (200–100 K)			
Axis 1	89 (2)	53 (3)	39 (3)
Axis 2	68 (6)	41 (4)	126 (4)
Axis 3	22 (6)	106 (5)	102 (4)

ture compression was observed. At temperatures between 225 and 200 K a phase transition occurred with a discontinuity in cell parameters and volume ($\Delta V/V$ = −2.66% referring to 300 K; Fig. 2). The transition was reversible with a small hysteresis, the reverse transformation taking place between 225 and 250 K. The space group changed from $P2_1/c$ [ambient-temperature phase (I)] to $P\bar{1}$ [low-temperature phase (II); Table 1], but no proton transfer between glutaric acid and glycine occurred (Fig. 1), and the hydrogen-bond network was basically preserved (Fig. 3). The conformation of every second glutaric acid molecule changed as a result of the phase transition, Z' increasing from 1 to 2 on cooling (Fig. 3). The main differences are related to changes in torsion angles O4—C3—C4—C5 [34.2 (2)° in the high-temperature phase (I), 80.7 (2)° in molecule 1 of the low-temperature phase (II), and 37.5 (3)° in molecule 2 of the low-temperature phase (II)] and C4—C5—C6—C7 [169.30 (14)° in the high-temperature phase (I), 75.0 (2)° in molecule 1 of the low-temperature phase (II), and 168.16 (18)° in molecule 2 of the low-temperature phase (II)] on cooling from 225 to 200 K. The two symmetry-independent glycine molecules in a unit cell still had very similar geometries (Fig. 3).

The anisotropy of strain on cooling before and after the phase transition point was compared in relation to the main structure-forming units and directions of hydrogen bonds in the structures. In the two phases all the contacts are heteromolecular; the molecules of glutaric acid alternate with glycine zwitterions to form main ring motifs consisting of four molecules linked *via* two types of hydrogen bond – O—H···O and N—H···O, $R_4^2(8)$, $R_4^4(18)$, $R_4^4(23)$ (Fig. 3). As phase (I) was cooled its structure compressed anisotropically, the softest direction being approximately normal to the mean planes of the $R_4^4(23)$ ring motifs and normal to the packages formed by glycine and glutaric acid molecules in [100] planes (Fig. 3). The structure was much more rigid in the directions within the mean planes of the ring motifs $R_4^4(23)$ formed by glycine and glutaric acid molecules (Figs. 3 and 4). Parameters characterizing linear strain along the principal axes of strain ellipsoid are summarized in Table 2 [phase (I) cooled from 300 to 225, and phase (II) from 200 to 100 K] and Fig. 5. During the phase transition on cooling between the temperatures 225 and 200 K, the dimensions of cell parameters ***b*** and ***c*** decreased 3.09 and 0.78%, respectively, while parameter ***a*** increased 0.55% (Figs. 2 and 3). The anisotropy of strain of phase (II) on further cooling after the phase transition was quite similar to that of phase (I): the structure of phase (II) was also most compressible in the direction normal to the $R_4^4(23)$ ring motifs, and was more rigid in the mean plane of these ring motifs (Figs. 4 and 5). At the same time, the principal axes 1 and 2 in phase (II), remaining in the mean plane of the ring motifs $R_4^4(23)$ containing four molecules, rotated with respect to the orien-

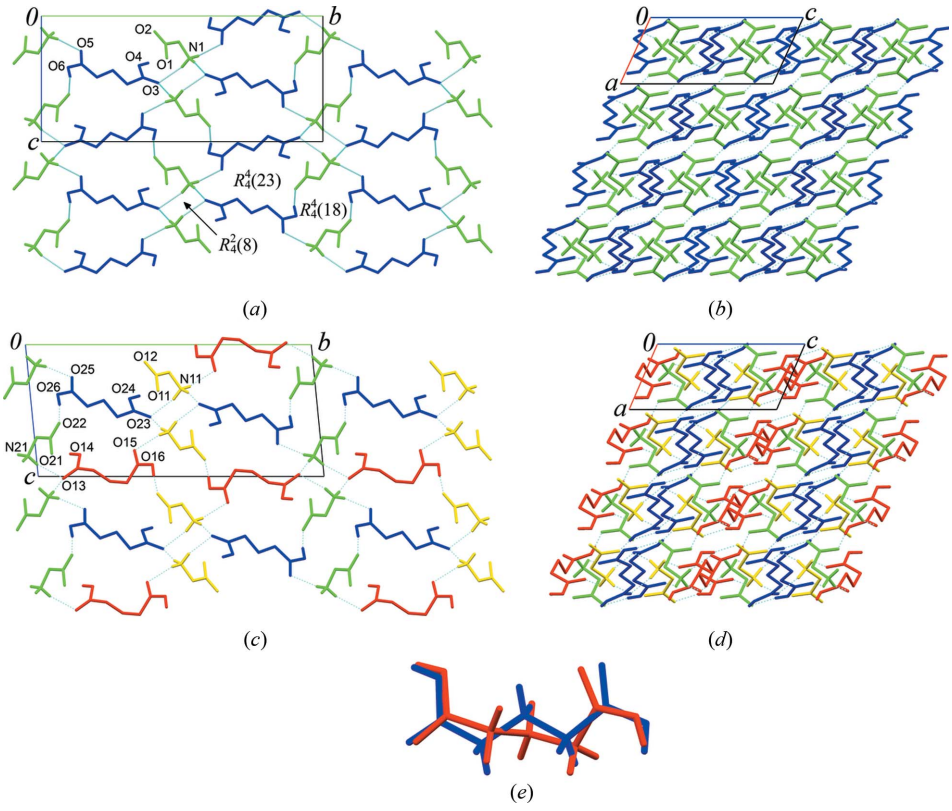

Figure 3
Fragments of the crystal structures of phases (I) (*a* and *b*) and (II) (*c* and *d*) of a glutaric acid–glycine co-crystal. Symmetry-independent molecules are shown by different colours. H atoms which are not involved in hydrogen bonds and are hanging contacts are omitted for clarity. The result of overlaying the two glutaric acid molecules with different conformations in phase (II) is shown in (*e*).

tation of molecules in phase (I) at about 30°. In phase (I) the principal axis 1 was directed along chains $C_4^3(13)$ containing N—H···O and short O—H···O hydrogen bonds [N1—H1*B*···O3 $(1-x, -\frac{1}{2}+y, \frac{1}{2}-z)$, N1—H1*C*···O3 $(x, \frac{3}{2}-y, \frac{1}{2}+z)$, N1—H1*A*···O5, O6—H6···O2 $(1-x, 1-y, -z)$], whereas principal axis 2 was directed along hydrogen-bonded chains $C_2^2(10)$ formed by N—H···O hydrogen bonds [N1—H1*A*···O5, N1—H1*B*···O3 $(1-x, -\frac{1}{2}+y, \frac{1}{2}-z)$]. In phase (II) axis 1 has no clear coincidence with hydrogen-bonded chains in the structure, but is close to chain $C_4^4(23)$ [formed by N11—H11*B*···O23 $(1-x, 1-y, 1-z)$, O16—H16···O12 $(1-x, 1-y, 2-z)$, N21—H21*C*···O13 $(x, 1+y, z)$, N21—H21*A*···O25], which is directed approximately along bisecting lines between axes 1 and 2; axis 2 was directed along the chain $C_4^4(23)$ formed by other types of N—H···O and O—H···O hydrogen bonds [N11—H11*C*···O23, N11—H11*A*···O15, N21—H21*B*···O13 $(1-x, 1-y, 2-z)$, O26—H26···O22 $(1-x, 2-y, 1-z)$, see Figs. 3*a* and *c*, and 4]. The directions of principal axes 3 in both phases agreed with a large decrease in the interlayer distance (Figs. 3*b* and *d*, and 4).

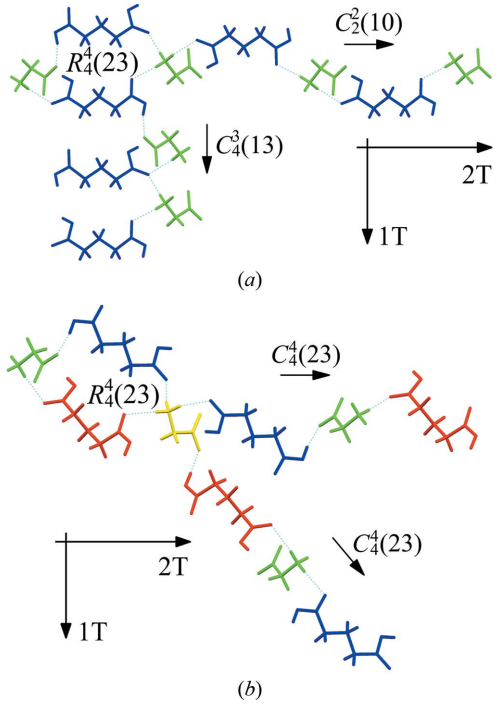

Figure 4
The orientation of the principal axes of strain ellipsoid with respect to selected hydrogen-bonded motifs in phases (I) and (II) of a glutaric acid–glycine co-crystal. The principal axis 3 of the strain ellipsoid is normal to the plane of the figure, axes 1 and 2 are in the plane of the figure.

No significant changes in the general network of hydrogen bonds occurred during the phase transition (Fig. 3). One can suppose that it is the conservation of the hydrogen-bond network that makes it possible for a crystal to remain undamaged when brought several times through the phase transition point on cooling and on reverse heating, with the hydrogen bonds acting as 'springs'. The major changes were related to the N—H···O and one of the two types of O—H···O hydrogen bonds.

The number of *symmetrically independent* hydrogen bonds formed by each donor in the crystal structure increased twice as a result of the phase transition on cooling. Thus, two non-equivalent hydrogen bonds in phase (II) substituted two symmetrically equivalent hydrogen bonds originally present in phase (I). The lengths and the compressibility of N—H···O hydrogen bonds in two different phases changed after the phase transition (Fig. 6). Interestingly, the hydrogen bond O6—H6···O2 $(1-x, 1-y, -z)$ with an unusual geometry (in which the H atom attached to O—H of a carboxylic group points 'further away', see Fig. 1) did not change much during the phase transition. In other words, two symmetrically different bonds with 'unusual' geometry in phase (II) were formed from two equal hydrogen bonds of similar geometry in phase (I). There are several examples (> 150) for which such 'unusual' bonds are found in the solid state in the CSD [*e.g.* refcodes DOGBOR (Ibrahem *et al.*, 2008), EMUFEX (Zheng *et al.*, 2003)] and their occurrence may be related to some packing restrictions in order for intermolecular O—H···O bonds to be possible. Short O6—H6···O2 $(1-x, 1-y, -z)$ hydrogen bonds were only slightly (if at all) compressed on cooling in phase (I), but 'expanded' in a discontinuous way during the phase transition, after which two non-equivalent and almost uncompressible hydrogen bonds of different strength substituted two equivalent bonds in phase (I) [O16—H16···O12 $(1-x, 1-y, 2-z)$ and O26—H26···O22 $(1-x, 2-y, 1-z)$]. The O4—H4···O1 $(-z, \frac{1}{2}+y, \frac{1}{2}-z)$ hydrogen bonds in phase (I) also compressed on cooling in the ambient-temperature phase, but after the phase

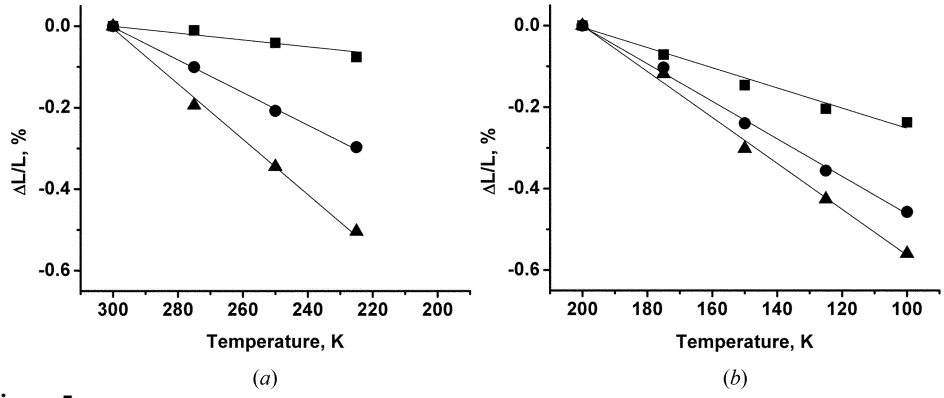

Figure 5
Linear strain in the directions of principal axes of strain ellipsoid *versus* temperature in phases (I) (*a*) and (II) (*b*) of glutaric acid–glycine co-crystal. For both structures the values of linear strain along the principal axes of strain tensor [1 (minimum linear size of strain ellipsoid), 2 (normal to 1 and 3), 3 (maximum linear size of train ellipsoid)] are plotted as squares, circles and triangles, respectively. Ambient temperature is taken as a reference point for phase (I); 200 K for phase (II).

transition all the originally equal bonds of this type became substituted for two non-equivalent types of hydrogen bonds with different strength and behavior on further cooling: the slope of the temperature dependence of the O24—H24···O11 $(-1+x, y, z)$ bond in phase (II) remained the same, as it was for the corresponding hydrogen bond O4—H4···O1 $(-z, \frac{1}{2}+y, \frac{1}{2}-z)$ in phase (I); however, in contrast to that, the slope for O14—H14···O21 $(1+x, -1+y, z)$ bond-length dependence on temperature in phase (II) was noticeably steeper than that for the related bond O4—H4···O1 $(-z, \frac{1}{2}+y, \frac{1}{2}-z)$ in phase (I). The main changes in the lengths of the hydrogen bonds, however, were observed for the N—H···O hydrogen bonds (Fig. 6). During the phase transition on cooling, the lengths of some of the N—H···O hydrogen bonds [N1—H1*A*···O5, N1—H1*C*···O3 $(x, \frac{3}{2}-y, \frac{1}{2}+z)$] increased, whereas that of the N1—H1*B*···O3 $(1-x, -\frac{1}{2}+y, \frac{1}{2}-z)$ bond decreased. The lengths of the N11—H11*B*···O23 $(1-x, 1-y, 1-z)$ and N21—H21*B*···O13 $(1-x, 1-y, 2-z)$ hydrogen bonds after the phase transition on cooling remained almost equal, although these bonds were no longer equivalent in phase (II).

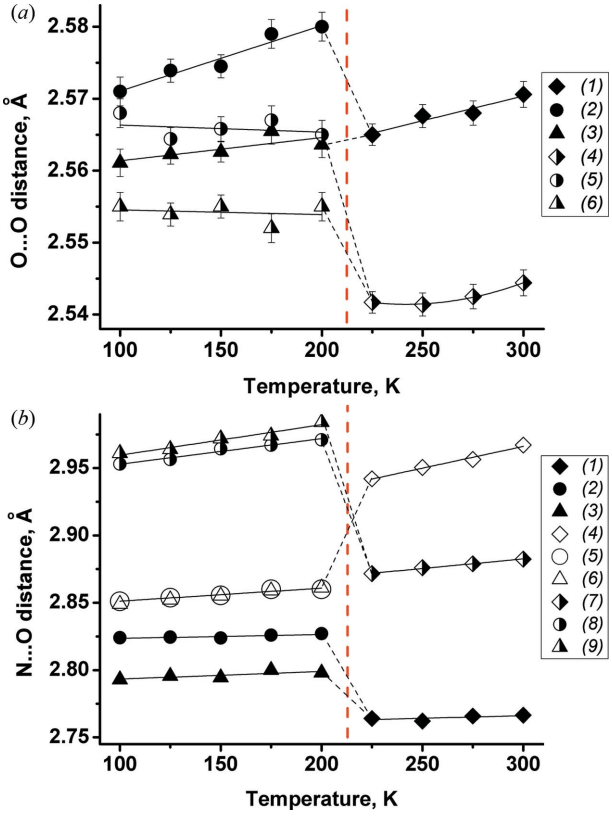

Figure 6
Changes in the donor–acceptor distances in the O—H···O (*a*) and N—H···O (*b*) hydrogen bonds in a glutaric acid–glycine co-crystal on cooling. Numbering of bonds for (*a*): (1) O4—H4···O1 $(-x, \frac{1}{2}+y, \frac{1}{2}-z)$, (2) O14—H14···O21 $(1+x, -1+y, z)$, (3) O24—H24···O11 $(-1+x, y, z)$, (4) O6—H6···O2 $(1-x, 1-y, -z)$, (5) O16—H16···O12 $(1-x, 1-y, 2-z)$, (6) O26—H26···O22 $(1-x, 2-y, 1-z)$. Numbering of bonds for (*b*): (1) N1—H1*A*···O5, (2) N11—H11*A*···O15, (3) N21—H21*A*···O25, (4) N1—H1*B*···O3 $(1-x, -\frac{1}{2}+y, \frac{1}{2}-z)$, (5) N11—H11*B*···O23 $(1-x, 1-y, 1-z)$, (6) N21—H21*B*···O13 $(1-x, 1-y, 2-z)$, (7) N1—H1*C*···O3 $(x, \frac{3}{2}-y, \frac{1}{2}+z)$, (8) N11—H11*C*···O23, (9) N21—H21*C*···O13 $(x, 1+y, z)$. Error bars for N···O distances do not exceed symbol size.

One of the interesting features of the phase transition is that every second glutaric acid molecule changes its conformation (Fig. 3). Examples of an increase in the number of molecules in the asymmetric unit related to conformational polymorphic transitions have been reported previously for a number of organic and coordination compounds (Drebushchak *et al.*, 2009, 2011*a*,*b*; Görbitz, 2011; Siegler & Stavitski, 2010) having flexible molecules with low barriers separating different conformers,. An increase in the number of molecules in the asymmetric unit often does not require a substantial change in the topology of hydrogen bonding in the crystal and is a favorable option for increasing the packing density. It is difficult to say whether conformational changes induce a distortion of the geometric parameters of at least some of the hydrogen bonds in the basically preserved hydrogen-bond network or *vice versa*. One can imagine that an increase in packing density is the main driving force. The hydrogen bonds 'hold' the whole structure as 'springs', whereas the conformational changes and a slight distortion of individual hydrogen bonds interplay to let the molecules form an optimum packing.

3.2. Raman spectroscopy

The phase transition also manifested itself clearly in the single-crystal polarized Raman spectroscopy experiments (Fig. 7). At temperatures below 220 K new bands appeared in the spectra in intermolecular as well as in intramolecular regions. This is related to a general lowering of the symmetry of the crystal structure from monoclinic ($P2_1/c$) to triclinic ($P\bar{1}$; intermolecular vibrations) and to the presence of glutaric acid molecules in a new conformation after the phase transition on cooling (intramolecular vibrations). Changes in the hydrogen-bond network also lead to changes in the spectra, especially in the intensity of some bands. The NH_3 and CO_2 torsion vibrations were especially informative since they are very sensitive to the structural transformations and are well separated from other types of vibrations.

The CO_2 torsion vibrations observed in the range 130–190 cm^{-1} (Kolesov & Boldyreva, 2011) can be considered. One can see (Fig. 7*a*) that the number of vibration modes increased twice in the low-temperature phase compared with the ambient-temperature phase because the number of independent —COO groups also increased twice, from three to six.

The band at 517 cm^{-1} in phase (I) is related to NH_3 torsion vibrations (Bordallo *et al.*, 1998; Kolesov & Boldyreva, 2011). After the (I) → (II) phase transition three different lines appeared in the spectra, but only two of them, at 513 and 526 cm^{-1}, had the same intensity in the spectra with different polarizations and can, therefore, be assigned to NH_3 modes (Figs. 7*b*–*d*).[2] This confirms the conclusions from diffraction

[2] Intensity of NH_3 torsion vibrational modes should not depend on the polarization of the Raman spectrum, since the change in the polarization of these vibrations does not depend on direction

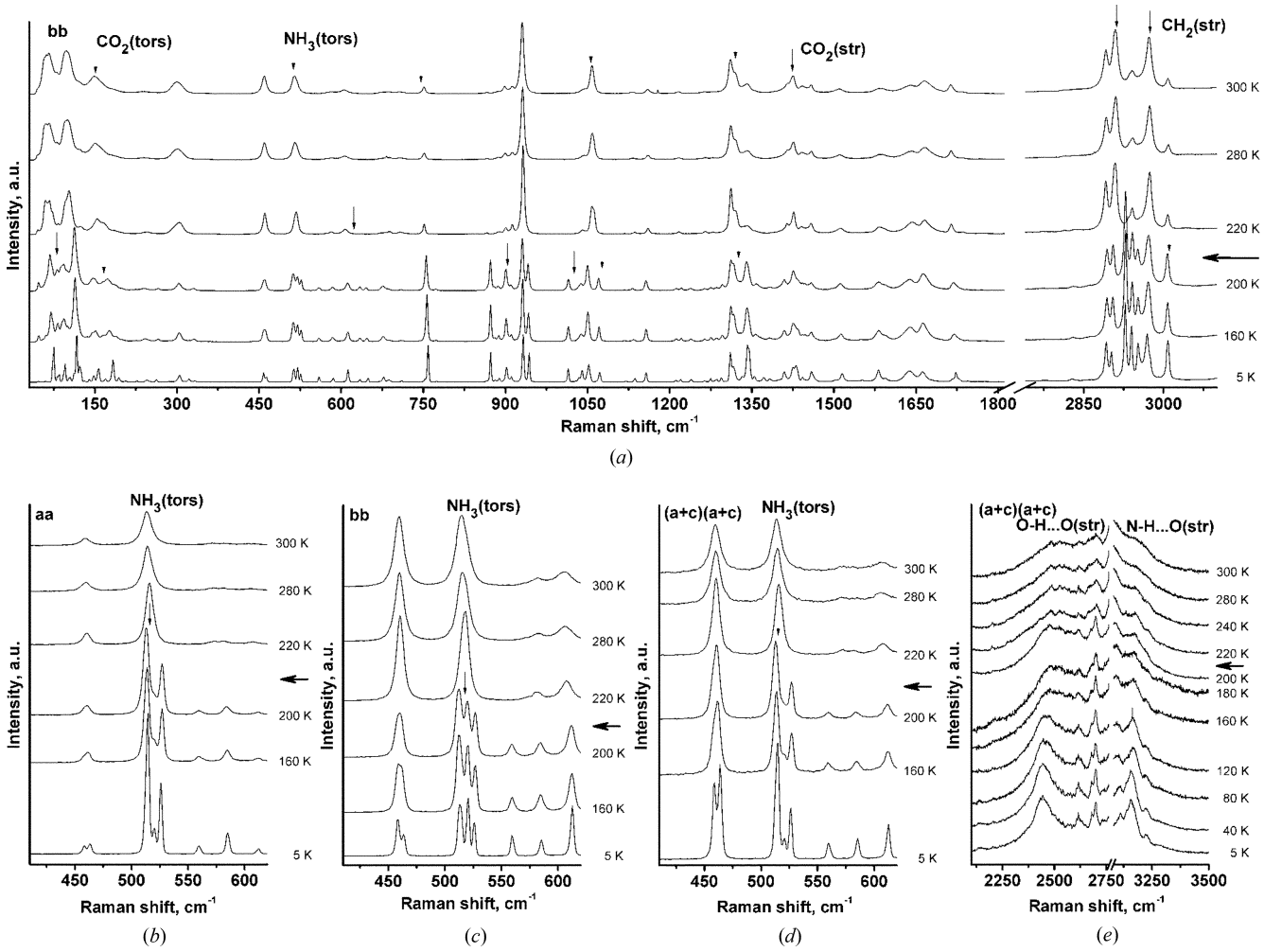

Figure 7
The fragments of polarized single-crystal Raman spectra of a glycine–glutaruc acid co-crystal. The bands changing on phase transition are indicated by small vertical arrows (large horizontal arrows show the borderline between the two phases). Polarization symbols are related to directions of crystallographic axes in phase (I).

experiments that in the low-temperature phase there are two types of NH_3 groups differing in crystalline environment.

Unfortunately, all the modes for O—H···O hydrogen bonds in the spectra overlap and form one broad band even at very low temperatures (Fig. 7*e*), mainly because of the similar donor–acceptor distances in different hydrogen bonds. Therefore, it was not possible to follow the vibrations of selected individual hydrogen bonds and to correlate their temperature dependences with changes in the interatomic distances, as has been done for some other amino acid salts (Zakharov *et al.*, 2011).

3.3. Differential scanning calorimetry

Thermal effects related to the phase transition have also been studied using DSC (Fig. 8). The first-order phase transition was observed both on single-crystalline and powder samples with no measurable particle size effect. Enthalpy of the transition was 897 ± 40 J mol^{-1} for sample 1 (three crystals) and 933 ± 40 J mol^{-1} for sample 2 (powder; Fig. 8). The DSC peak shape is typical of a first-order solid-solid phase transition, with a sharp increase at the beginning and a logarithmic relaxation at the end (Drebushchak, 2012). This agrees perfectly well with other obvious indications of the first-order type: a jumpwise change in cell parameters and volume, the hysteresis (Clark *et al.*, 1994; Herbstein, 2006, Tolédano *et al.*, 1998). Comparison of the DSC curves measured in several cooling–heating cycles for the same crystal (sample 3, Fig. 8) has shown not only the presence of a significant hysteresis, but also the dispersion of the transformation temperatures for different domains of the same crystal. This phenomenon is common for first-order phase transitions and has been reported earlier (see *e.g.* Boldyreva *et al.*, 2003, 2004; Minkov *et al.*, 2011). The hysteresis value observed for the glutaric acid–glycine co-crystals was not very large compared with some other examples described in the literature. For DL-cysteine, for example, the difference between the values obtained for different samples in different experiments exceeded 100 K (Minkov *et al.*, 2009). The transformation temperatures measured in X-ray diffraction and DSC experiments were in the same temperature range (218–228 K), but did not coincide. This is typical for first-order phase

transitions in the solid state and is related to kinetic effects, which are also responsible for the hysteresis and for the observed dispersion in the transformation in different crystal parts. Sometimes, intermediate phases can be detected on variation of cooling–heating rate or, on the contrary, a phase is 'overjumped' (see Siegler *et al.*, 2011 as a recent example). However, such phenomena have not been observed in our experiments with glutaric acid–glycine co-crystals.

4. Conclusions

The present study reports a new example of a single-crystal to single-crystal phase transition on cooling in a molecular co-crystal. In contrast to several previously studied systems (Asaji *et al.*, 2007; Grobelny *et al.*, 2011; Majerz *et al.*, 1997), temperature variation does not induce any proton transfer between the components which would give a salt. The packing density increases on cooling as a result of a conformational change in every second molecule of one of the components – glutaric acid, so that the number of molecules in the asymmetric unit increases and the space-group symmetry lowers. Similarly to that observed previously in the polymorphs of chlorpropamide (Drebushchak *et al.*, 2009, 2011*a*) and tolbutamide (Drebushchak *et al.*, 2011*b*), the conformational transformation does not require any dramatic changes in the hydrogen-bond network: the topology is preserved, although the bond lengths are changed and some of the bonds become non-equivalent. This may explain why single crystals do not break when brought repeatedly through the phase transition point in multiple cooling–heating cycles, if they are small enough (~ 0.4 mm). Larger (~ 3 mm) crystals do break on cyclic cooling–heating, since a mere distortion of hydrogen bonds in this case is not sufficient for stress relaxation, and other mechanisms involving dislocations, domain boundaries and other extended defects may come into play. The transition occurs both in single crystals and in powder samples, shows no pronounced particle size effect, and manifests itself in Raman spectra and in DSC experiments. Different crystallites/crystalline domains undergo the transition at slightly different temperatures.

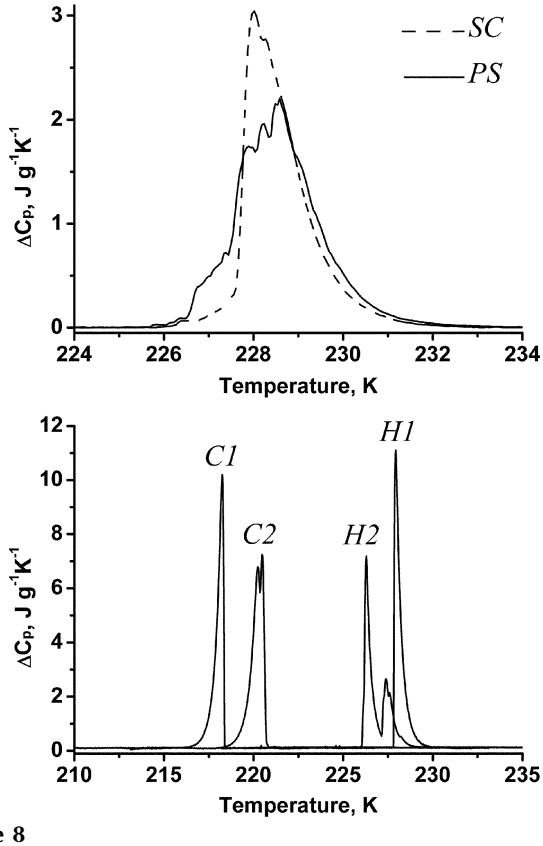

Figure 8
DSC curves of glutaric acid–glycine co-crystals at 6 K min^{-1}: (SC) three single crystals, sample 1 (PS), powder sample, sample 2, and at 3 K min^{-1} with two cooling/heating cycles, sample 3: (C1) cooling 1, (H1) heating 1, (C2) cooling 2, (H2) heating 2.

The study was supported by the RFBR grant # 10-03-00252, and the Programs of RAS ## 24.38 and 5.6.4.

References

Allen, F. H. (2002). *Acta Cryst.* B**58**, 380–388.
Allen, F. H., Johnson, O., Shields, G. P., Smith, B. R. & Towler, M. (2004). *J. Appl. Cryst.* **37**, 335–338.
Asaji, T., Seliger, J., Žagar, V., Sekiguchi, M., Watanabe, J., Gotoh, K., Ishida, H., Vrtnik, S. & Dolinšek, J. (2007). *J. Phys. Condens. Matter*, p. 19 art. No. 226203.
Boldyreva, E. V., Drebushchak, V. A., Drebushchak, T. N., Paukov, I. E., Kovalevskaya, Yu. A. & Shutova, E. S. (2003). *J. Therm. Anal.* **73**, 419–428.
Boldyreva, E. V., Drebushchak, V. A., Paukov, I. E., Kovalevskaya, Y. A. & Drebushchak, T. N. (2004). *J. Therm. Anal. Calorim.* **77**, 607–623.
Bordallo, H. N., Barthes, M. & Eckert, J. (1998). *Physica B*, **241**, 1138.
Casati, N., Macchi, P. & Sironi, A. (2009). *Chem Commun.* **19**, 2679–2681.
Childs, S. L., Stahly, G. P. & Park, A. (2007). *Mol. Pharm.* **4**, 323–338.
Chitra, R., Thiruvenkatam, V., Choudhury, R. R., Hosur, M. V. & Row, T. N. G. (2006). *Acta Cryst.* C**62**, o274–o276.
Clark, J. B., Hastie, J. W., Kihlborg, L. H. E., Metselaar, R. & Thackeray, M. M. (1994). *Pure Appl. Chem.* **66**, 577–594.
Drebushchak, V. A. (2012). *J. Therm. Anal. Calorim.*, DOI: 10.1007/s10973-012-2216-7.
Drebushchak, T. N., Chesalov, Y. A. & Boldyreva, E. V. (2009). *Acta Cryst.* B**65**, 770–781.
Drebushchak, T. N., Drebushchak, V. A. & Boldyreva, E. V. (2011*a*). *Acta Cryst.* B**67**, 163–176.
Drebushchak, T. N., Pankrushina, N. A. & Boldyreva, E. V. (2011*b*). *Dokl. Phys. Chem.* **437**, 61–64.
Fleck, M. & Petrosyan, A. M. (2010). *J. Cryst. Growth*, **312**, 2284–2290.
Görbitz, C. H. (2011). *J. Phys. Chem. B*, **115**, 2447–2453.
Grobelny, P., Mukherjee, A. & Desiraju, G. R. (2011). *CrystEngComm*, **13**, 4358–4364.
Hazen, R. & Finger, L. (1982). *Comparative Crystal Chemistry. Temperature, Pressure, Composition and Variation of the Crystal Structure.* New York: Wiley.
Herbstein, F. H. (2006). *Acta Cryst.* B**62**, 341–383.
Ibrahem, I., Hammar, P., Vesely, J., Rios, R., Eriksson, L. & Córdova, A. (2008). *Adv. Synth. Catal.* **350**, 1875–1884.
Kolesov, B. A. & Boldyreva, E. V. (2011). *J. Raman Spectrosc.* **42**, 696–705.
Losev, E. A., Zakharov, B. A., Drebushchak, T. N. & Boldyreva, E. V. (2011). *Acta Cryst.* C**67**, o297–o300.

Macrae, C. F., Bruno, I. J., Chisholm, J. A., Edgington, P. R., McCabe, P., Pidcock, E., Rodriguez-Monge, L., Taylor, R., van de Streek, J. & Wood, P. A. (2008). *J. Appl. Cryst.* **41**, 466–470.
Majerz, I., Malarski, Z. & Sobczyk, L. (1997). *Chem. Phys. Lett.* **274**, 361–364.
Minkov, V. S., Drebushchak, V. A., Ogienko, A. G. & Boldyreva, E. V. (2011). *CrystEngComm*, **13**, 4417–4426.
Minkov, V. S., Tumanov, N. A., Kolesov, B. A., Boldyreva, E. V. & Bizyaev, S. N. (2009). *J. Phys. Chem. B*, **113**, 5262–5272.
Natarajan, S., Kalyanasundar, A., Suresh, J., Dhas, S. A. M. B. & Lakshman, P. L. N. (2009). *Acta Cryst.* E**65**, o462.
Rajagopal, K., Krishnakumar, R. V., Mostad, A. & Natarajan, S. (2001). *Acta Cryst.* E**57**, o751–o753.
Riscob, B., Shakir, Mond, Kalyana Sundar, J., Natarajan, S., Wahab, M. A. & Bhagavannarayana, G. (2011). *Spectrochim. Acta Part A*, **78**, 543–548.
Sekhon, B. S. (2009). *Ars Pharm.* **50**, 99–117.
Shan, N. & Zaworotko, M. J. (2008). *Drug Discovery Today*, **13**, 440–446.
Sheldrick, G. M. (2008). *Acta Cryst.* A**64**, 112–122.
Siegler, M. A., Hao, X., Parkin, S. & Brock, C. P. (2011). *Acta Cryst.* B**67**, 486–498.
Siegler, M. A. & Stavitski, E. (2010). *Acta Cryst.* B**66**, 430–440.
Spek, A. L. (2009). *Acta Cryst.* D**65**, 148–155.
Stoe & Cie (2006). *X-AREA* and *X-RED32*. Stoe and Cie, Darmstadt, Germany.
Subha Nandhini, M., Krishnakumar, R. V. & Natarajan, S. (2001). *Acta Cryst.* C**57**, 115–116.
Tolédano, J.-C., Glazer, A. M., Hahn, Th., Parthé, E., Roth, R. S., Berry, R. S., Metselaar, R. & Abrahams, S. C. (1998). *Acta Cryst.* A**54**, 1028–1033.
Tumanov, N. A., Boldyreva, E. V. & Shikina, N. E. (2010). *Acta Cryst.* C**66**, o279–o283.
Zakharov, B. A., Kolesov, B. A. & Boldyreva, E. V. (2011). *Phys. Chem. Chem. Phys.* **13**, 13106–13116.
Zheng, Y.-Q., Lin, J.-L. & Kong, Z.-P. (2003). *Polyhedron*, **22**, 2699–2708